

^{18}F -FAraG PET for CD8 Profiling of Tumors and Assessment of Immunomodulation by Chemotherapy

Jelena Levi^{1*}, Samuel Goth¹, Lyna Huynh¹, Tina Lam¹, Tony L Huynh², Brailee Schulte², Juliet A Packiasamy¹

¹CellSight Technologies Incorporated, San Francisco, California; ²Department of Radiology and Biomedical Imaging, University of California, San Francisco, San Francisco, California;

*Corresponding Author

Jelena Levi, PhD

185 Berry street,

San Francisco, 94107, CA

Email: jlevi@cellsighttech.com

Running Title: [^{18}F]F-AraG for CD8 profiling of tumors

Financial statement: This work was supported by National Institutes of Health Grants NCI SBIR HHSN261201800024C (JL).

Conflict of Interest Statement: JL, SG, LH, TL and JP are or were employed by CellSight Technologies. CellSight Technologies Incorporated is commercializing [^{18}F]F-AraG as a PET tracer for evaluation of immune response in immunotherapy. No other potential conflicts of interest relevant to this article exist.

ABSTRACT

Majority of the clinical trials exploring various combinations of chemo- and immunotherapy rely on serial biopsy to provide information on immune response. The aim of this study was to assess the value of ^{18}F -FAraG as a non-invasive tool that could profile tumors based on the key players in adaptive antitumor response, CD8+ cells, and evaluate immunomodulatory effects of chemotherapy.

Methods. To evaluate the ability of ^{18}F -FAraG to report on the presence of CD8+ cells within the TME, we imaged a panel of syngeneic tumor models (MC38, CT26, LLC, A9F1, 4T1 and B16F10), and correlated the signal intensity with the number of lymphocytes found in the tumors. The capacity of ^{18}F -FAraG to detect immunomodulatory effects of chemotherapy, was determined by longitudinal imaging of tumor bearing mice (MC38, A9F1) undergoing two types of chemotherapy: oxaliplatin/cyclophosphamide, shown to induce immunogenic cell death and paclitaxel/carboplatin, reported to cause immunogenically silent tumor cell death.

Results. ^{18}F -FAraG revealed strikingly different uptake patterns in the tumor panel, which resembled cancer-immune phenotypes observed in the clinic. Statistically significant correlation was found between the ^{18}F -FAraG signal and the number of PD-1 positive CD8+ cells isolated from the tumors ($r^2=0.528$, $p<0.0001$). In the MC38 model, paclitaxel/carboplatin did not result in appreciable change in signal post therapy (1.69 ± 0.25 vs. 1.50 ± 0.33 %ID/g), but oxaliplatin/cyclophosphamide treatment led to close to 2.4 fold higher ^{18}F -FAraG signal (1.20 ± 0.31 vs. 2.84 ± 0.93 %ID/g). The statistically significant increase in signal post oxaliplatin/cyclophosphamide was also observed in A9F1 model (0.95 ± 0.36 vs. 1.99 ± 0.54 %ID/g).

Conclusion. The ability of ^{18}F -FAraG PET to assess the location and function of CD8+ cells, as well immune activity within tumors post immune priming therapy warrants further investigation into its utility for patient selection, evaluation of optimal time to deliver immunotherapies, and assessment of combinatorial therapy approaches.

INTRODUCTION

Tumor microenvironment (TME) consists of multiple, mutually interacting components that collectively form an immunosuppressive, tumor-promoting environment that affects the tumor's aggressiveness, metastatic potential and response to therapy (1). The impressive clinical successes achieved with the use of checkpoint inhibitors convincingly illustrate the importance of TME modulation in cancer treatment (2). However, objective and durable responses have to date been attained only in a relatively small fraction of patients with solid tumors. Although the exact reasons for low response rates are yet to be defined, the evidence supports the significance of weak immune activity within tumors. A robust intratumoral infiltration by immune cells has been correlated with good clinical outcome in colorectal cancer, melanoma, breast, bladder, ovarian, lung and other cancers (3). Of the three basic cancer-immune phenotypes found across different tumor types-immune inflamed, immune excluded and immune desert - inflamed tumors show the best response to immunotherapy (4).

To enable successful immunotherapy in a larger population of patients, many novel therapies aim to create a "hot" immune environment conducive to successful immunotherapy (5). The discovery of the immune response that results from chemotherapy-induced tumor cell death, termed immunogenic cell death (6), has sparked interest in harnessing chemotherapy's immunomodulatory effects for possible synergistic combinations with immunotherapeutics (7,8). Immunogenic cell death is signified by a series of processes that allow chemotherapeutics to act as *in situ* vaccine, generating innate and adaptive immune responses. Cell surface translocation of proteins associated with dying cells, such as calreticulin and heat shock proteins, as well as the release of other danger-associated molecular patterns, such as high-mobility group box 1 and adenosine triphosphate, stimulate mobilization of dendritic cells, engulfment of apoptotic cells, antigen processing and presentation, and activation of T cells (8).

The number of trials that test PD-1/PD-L1 checkpoint inhibitor therapy in combination with chemotherapy far exceed immunotherapy combination trails with any other type of cancer treatment (9). Majority of these trials rely on multiple biopsy specimens acquired before and during chemo-immunotherapy treatment to provide

information on the changes in the immune contexture (10). However, invasiveness and sampling variability diminish the utility of serial biopsy in immunomonitoring. Herein, we assess the value of using ^{18}F -FAraG, a PET agent relatively specific for activated T cells (11-13), as a non-invasive tool that could profile tumors based on the key players in adaptive antitumor response, CD8+ cells, and evaluate immunomodulatory effects of chemotherapy.

MATERIALS AND METHODS

Cell Lines and Tumor Models

Lewis Lung Carcinoma (LLC), colon adenocarcinoma (MC38), colorectal carcinoma (CT26), melanoma (B16F10), and mammary (4T1) cell lines were purchased through ATCC (Virginia, USA). With the help of Dr Esteban Celis (Augusta University, Augusta, GA), Lewis Lung Carcinoma subclone (A9F1) cells were obtained from Dr. Lea Eisenbach (Weizmann Institute of Science, Rehovot, Israel)(14). A9F1, LLC, MC38 and B16F10 cells were cultured in Dulbecco's Modified Eagle Medium (GE Healthcare-Hyclone, Utah, USA) with 10% Fetal Bovine Serum (GE Healthcare) and 1% Penicillin:Streptomycin solution (GE Healthcare). CT26 and 4T1 cells were cultured in RPMI 1640 (GE Healthcare) containing 10% Fetal Bovine Serum, 1% MEM Non-essential Amino Acids (Corning, Virginia, USA), 1% Sodium Pyruvate (Corning) and 0.5% of PAGE β -Mercaptoethanol. Tumor volume was determined by measuring two opposing diameters and using the formula $V=\pi/6(\text{length} \times \text{width})^{3/2}$.

Six to eight-week-old C57BL/6 (n=16) and Balb/C (n=8) (Jackson Laboratory, USA) were shaved at left flank two days prior to injection and monitored for irritation. C57BL/6 mice were subcutaneously injected into the left flank with the following: 2 million A9F1 cells, 0.5 million MC38 cells, 0.3 million LLC cells and 0.5 million B16F10 cells. Balb/C mice were subcutaneously injected into the left flank with 0.75 million CT26 cells and 0.5 million 4T1 cells.

All animal care and experiments were conducted at the University of California, San Francisco (UCSF) facilities that are accredited by the American Association for Accreditation of Laboratory Animal Care. All animal studies were performed in accordance with UCSF IACUC approval.

¹⁸F-FArA G Imaging of Tumor Model Panel

Tumor bearing mice (MC38, CT26, LLC, A9F1, 4T1 and B16F10, n=4 for each group) were imaged 14 days post tumor implantation. All images were performed using a dedicated small animal PET/CT (Inveon, Siemens Medical Solutions, Malvern, PA). ¹⁸F-FArA G (5.5-7.4 MBq within 100-200 μ L sterile saline) was administered intravenously via tail vein under anesthesia (2-2.5% isoflurane) to all animals. Uptake time of 60 minutes for the animals was followed before the start of every scan. During the uptake time, animals were kept awake within their cages over a temperature-controlled heating pad at 37°C, as necessary. 15-minute static PET data was acquired for all animals followed by CT for anatomical reference under anesthesia (2-2.5% isoflurane). Region-of-interest (ROI) analysis of the PET/CT data was performed using VivoQuant 3.5 software (Invivo, Boston MA). For the lymph nodes, the ROIs were defined by placing a fixed volume sphere at the anatomically correct location. Partial volume correction was not performed. The percentage of injected dose per gram was calculated for each ROI.

¹⁸F-FArA G Imaging of Tumor Bearing Mice Undergoing Chemotherapy Treatment

Mice carrying MC38 (n=8), A9F1 (n=8) and 4T1 (n=8) tumors were split into two sets. One group of mice (n=4) were treated with oxaliplatin (2.5 mg/kg of body weight)-cyclophosphamide (50 mg/kg of body weight) and the other set with paclitaxel (10 mg/kg of body weight) and carboplatin (10 mg/kg of body weight). All drugs were purchased from TCI America. Mice were imaged periodically over the course of 2 weeks, one day before the start of therapy and then 3 and 6 days after the first chemotherapy administration, and 3 days after the second chemotherapy administration (Supplemental Fig1). PET imaging and analysis was performed as described above for the tumor model panel.

FACS Analysis

Mice were euthanized 24 hours after the last imaging timepoint. Tumors were excised and single cell suspensions were prepared using gentleMACS Octo Dissociator (Miltenyi Biotec) according to the manufacturers' instructions. Tumors were dissociated by a combination of mechanical dissociation and enzymatic digestion (Mouse tumor

dissociation kit, 130-096-730, MACs Miltenyi Biotec). After dissociation, samples were passed through 70 μ m and 30 μ m cell strainers to remove any remaining larger particles from the single-cell suspension. For flow cytometry, an aliquot of each sample, containing one million cells, was transferred into a 12 \times 75-mm polystyrene tube and TruStain FcX™ (common epitope of CD16/CD32, BioXcell) was added to block non-specific binding. Cell surface staining with fluorescently labeled antibodies for various markers was performed in a staining buffer (PBS containing 0.5 % BSA and 0.02 % sodium azide) for 30 min at 4 °C. For FoxP3 staining, cells were washed with staining buffer, fixed and permeabilized (Foxp3 Transcription Factor Staining Buffer kit, eBioscience), and intracellularly stained with FoxP3 antibody. Cell viability for FACS was determined by staining primary isolated cells with an amine reactive dye (Violet Live/dead viability kit, Thermo Fisher, Waltham, MA) with 405/450nm ex/em maxima. The data were collected on a FACSARIA II or III and analyzed using FlowJo software (FlowJo, Ashland Oregon).

Additional information on the antibodies used are provided in the Supplemental Table 1.

RESULTS

¹⁸F-FAraG Reveals Distinct Patterns of Uptake in Different Tumor Types

To mimic the variations in cancer-immune phenotypes observed in the clinic, we created six syngeneic tumor models reported to have different immune contexture (15,16): colon (MC38 and CT26), lung (Lewis lung carcinoma, LLC and A9F1, an immunogenic Lewis lung clone), breast (4T1) and melanoma (B16F10). ¹⁸F-FAraG accumulation in tumors as well as in tumor draining lymph nodes (TDLN) varied not only between different tumor types but also between individual mice of the same tumor type (Figure 1). Qualitatively, ¹⁸F-FAraG revealed strikingly different intratumoral uptake patterns (Figure 1A): signal in the tumor core (MC38 and A9F1), signal encircling the tumor (CT26), signal at the tumor margin (half-moon signal in LLC and patchy signal in B16F10) and absence of signal (4T1).

Intratumoral signal intensity showed an expected variation between tumor types and individual mice (Figure 1B). The lowest signal was observed in 4T1 tumor bearing mice while mice carrying MC38, CT26 and A9F1 tumors showed the highest signal intensity. The differences in ¹⁸F-FAraG accumulation were also observed in the TDLNs (Figure 1B). While some mice showed strong intranodal signal (MC38, A9F1), in others (4T1, B16F10) only faint signal was observed in the TDLNs.

The Syngeneic Tumor Model Panel Captures Heterogeneity in CD4+ and CD8+ Contexture

To evaluate CD4+ and CD8+ contexture, tumors were excised one day after imaging and immune infiltrates isolated and analyzed. Similar to the immune variations observed in the clinic, the immune contexture in these preclinical models varied not only between different tumor types but also between individual mice with the same tumor type (Figure 2). As the sizes varied between different tumors types (Supplemental Fig. 2), the models were compared both in terms of the number of cells per gram of tumor (Figure 2A) and number of cells found in each tumor (Figure 2B). The highest density of total lymphocytes as well as CD4+ and CD8+ cells, believed to be crucial for tumor control,

was found in the smallest tumors, A9F1 (Figure 2A). In contrast, the highest number of lymphocytes were isolated from the largest tumors, 4T1 (Figure 2B). Interestingly, although abundant in 4T1 tumors, only a fraction of CD8+ cells expressed programmed cell death -1 (PD-1) (Figure 2C). In LLC and A9F1 tumors, over 97 % of CD8+ cells were found to be PD-1 positive, while in 4T1 tumors, less than 30 % of CD8 cells expressed PD-1. Although PD-1 expression alone cannot distinguish between exhausted and functional CD8 cells, in the context of rapidly growing tumors such as 4T1, the lack of PD-1 expression suggests impaired T cell activation rather than antigen clearance (17).

¹⁸F-FAraG Signal Correlates with the Number of PD-1 Positive CD8 Cells

To evaluate the ability of ¹⁸F-FAraG to report on the presence of CD8+ cells within the TME, the signal intensity was correlated with the number of lymphocytes found in the tumors (Figure 3). While ¹⁸F-FAraG intensity did not correlate with the number of total CD45+, CD11b+ (Supplemental Fig. 3) or CD8+ cells (Figure 3A) found in the tumor, statistically significant correlation was found with the number of PD-1 positive CD8+ cells (Figure 3B). It is interesting to note that excluding data from 4T1 tumors that showed low PD-1 expression indicative of dysfunction of T cell activation, resulted in a statistically significant correlation between the signal and number of CD8+ cells (Figure 3C).

¹⁸F-FAraG Can Evaluate Immunomodulatory Effects of Chemotherapy

To assess the ability of ¹⁸F-FAraG to detect immunomodulatory effects of chemotherapy, we performed longitudinal imaging of MC38 mice undergoing two types of chemotherapy oxaliplatin/cyclophosphamide, known to induce immunogenic cell death and paclitaxel/carboplatin, reported to cause immunogenically silent tumor death (18) (Supplemental Fig. 1). Although the signal did not change significantly after the first administration of either of the two chemotherapy combinations (Figure 4A panels P1 and P2), the second treatment with oxaliplatin/cyclophosphamide combination resulted in a dramatic change in the ¹⁸F-FAraG signal (post Tx panel). While in the paclitaxel/carboplatin group the signal did not change appreciably post therapy,

oxaliplatin/cyclophosphamide treatment led to close to 2.4 fold higher ^{18}F -FAraG signal (Figure 4B).

The increase in signal post chemotherapy was also observed in A9F1 bearing mice (Figure 5A). Although both chemotherapy regimens led to an increase in signal, only oxaliplatin-cyclophosphamide led to a statistically significant signal change (Figure 5B).

In contrast to the changes observed in MC38 and A9F1 tumors, the post therapy ^{18}F -FAraG signal in 4T1 tumors did not differ from the baseline signal for either of the two chemotherapy regimens, (Supplemental Fig. 4).

The Change in Immune Contexture Corresponded with the Observed Changes in the ^{18}F -FAraG Signal

One day after the final ^{18}F -FAraG scan, MC38 and A9F1 tumors were excised and tumor infiltrating lymphocytes isolated and characterized. Compared to paclitaxel/carboplatin, oxaliplatin/cyclophosphamide therapy led to an increase in total lymphocytes in both MC38 and A9F1 tumors. However, the effect on the number of CD4+ and CD8+ cells was different in these two tumor types. In the MC38 model, treatment with oxaliplatin/cyclophosphamide resulted in an increase in CD8+ cells, while in A9F1 tumors it had a larger effect on the number of CD4+ cells (Figure 6A). However, although the number of CD4+ cells in MC38 tumors was found to be similar in both treatment groups, further analysis of the CD4 cell subset revealed lower intratumoral abundance of regulatory CD4+FOXP3+ cells in mice treated with oxaliplatin/cyclophosphamide. Consequently, the ratio of effector CD8+ cells to regulatory CD4+FOXP3+, found to have prognostic significance (19), was 27-fold higher in the oxaliplatin/cyclophosphamide group compared to paclitaxel/carboplatin treated mice (Figure 6B). This striking difference in immune contexture agrees well with the statistically significant difference in signal between the groups of mice treated with different chemotherapy drugs (Figure 4B). Furthermore, in A9F1 model in which the difference between the two chemotherapy groups was not statistically significant (Figure 5B), no changes in ratio of CD8+ to CD4+FOXP3+ was recorded (Supplemental Fig. 5).

DISCUSSION

In contrast to the impressive strides in the development of novel immunotherapeutic approaches, immune biomarkers that enable patient selection, evaluation of therapy response, as well as the optimal time to start immunotherapy remain unsolved clinical challenges. As a non-invasive, whole body technique that can track biological processes, PET provides a strong framework for development of imaging biomarkers capable of evaluating complex immunological interplays.

Many efforts in imaging biomarker development focus on T cells, in particular CD8+ cells, as they play a central role in adaptive immune response and their presence in the TME largely indicates a positive prognosis (3). We and others have reported several T cell-based imaging biomarkers showing promise in predicting immunotherapy response(13,20-23). Here, we assessed the ability of ^{18}F -FAraG, a PET agent that preferentially accumulates in activated CD8+ T cells, to report on the CD8+ profile of tumors prior to starting any therapy and to track immunomodulation of the TME during immune priming by chemotherapy.

The six syngeneic models chosen to represent variations in cancer immune microenvironment observed in the clinic, showed expected immunological heterogeneity. Tumors differed in terms of the size, number and density of CD4+ and CD8+ cells. ^{18}F -FAraG imaging was able to successfully capture the diversity between tumor models. Interestingly, the patterns of signal location within tumors were highly reminiscent of the three basic cancer immune phenotypes: immune inflamed with signal in the core; immune excluded with signal at the margin; and immune desert with signal void. This capacity to report on the location of the immune infiltrates within tumors could allow non-invasive assessment of cancer immune phenotype, akin to immunoscore (24), and evaluation of T cell migration post therapy. Importantly, ^{18}F -FAraG scan agreed well with the CD8+ profile of the tumors. The lack of PD-1 expression isolated from 4T1 tumors well infiltrated with CD8+ cells, suggestive of the activation dysfunction, was reflected in the low signal in the tumor and the primary site of antigen presentation, TDLN. On the other hand, A9F1 tumors, abundant in PD-1 positive CD8+ cells showed high intratumoral and intranodal signal. The holistic assessment of not only presence but also functional status of

lymphocytes in both tumors and TDLNs may provide clues into different factors that can affect therapy outcome, such as metabolism or antigen recognition, and thus help in rational selection of combinatorial therapies (25,26).

The ability of ^{18}F -FAraG to provide the CD8+ status of tumors was demonstrated by correlating the tracer's intratumoral uptake with the number of CD8+ cells isolated from the tumors. Statistically significant correlation was found between the signal and the number of CD8+ PD-1+ cells, but not with the number of all lymphocytes isolated from the tumors. Although the correlation seems to be only moderate ($r^2= 0.528$, $p < 0.0001$) this is anticipated as the accumulation of ^{18}F -FAraG in T cells rests on its phosphorylation by kinases, whose activity depends on functional state of T cells (11,13,27). A meta-analysis of studies correlating tumor cell proliferation with ^{18}F -FDG uptake, whose mechanism of accumulation in cancer cells parallels that of ^{18}F -FAraG in activated T cells, found similar level of correlation for many tumor types (28). The correlation between ^{18}F -FAraG signal and intratumoral CD8+ PD-1+ cells could have significant clinical implications. A study investigating PD-1 expression of intratumoral CD8+ cells in a small cohort of patients with non-small cell lung cancer, found the presence of tumor infiltrating lymphocytes with high PD-1 expression to be strongly predictive of response to PD-1 therapy and survival, thus indicating that the quantification of this CD8+ subset may serve as a promising proxy for the anti-tumor T cell potential (29).

Longitudinal imaging of chemotherapy treatment clearly demonstrated the ability of ^{18}F -FAraG to evaluate immunomodulatory effect of chemotherapy. Oxaliplatin/cyclophosphamide treatment led to statistically significant increases in signal in MC38 and A9F1 bearing mice. Interestingly, there were notable differences between the two models. In the MC38 model, the striking 2.4-fold increase in post therapy signal was observed only in mice treated with oxaliplatin/cyclophosphamide, while the signal post paclitaxel/carboplatin therapy did not change appreciably. In the A9F1 model, both chemotherapy combinations led to a change in the signal, but only oxaliplatin/cyclophosphamide treatment resulted in a statistically significant, 2-fold signal increase.

These imaging results corresponded to the differences in the TME that were detected between chemotherapies and tumor models. Oxaliplatin/cyclophosphamide resulted in the increase in lymphocytes for both tumor types, but the effect on the CD4 and CD8 subsets depended on the tumor type. In the MC38 colon cancer model, oxaliplatin/cyclophosphamide led to a 27-fold higher ratio of CD8+ to CD4+FOXP3+ cells compared to paclitaxel/carboplatin, indicating a more immune active TME. Supportive of these findings, in metastatic colorectal cancer patients low dose cyclophosphamide induced Treg depletion and boosted antitumor immunity (30).

CONCLUSION

Our data suggest ¹⁸F-FARA-G PET is a promising tool for CD8 profiling of the tumors and evaluation of chemotherapy-based immune induction strategies. The findings raise a question of the threshold signal and/or signal change that is needed for adequate immune priming. That question, along with the relevance of the type of cellular changes occurring in the TME on the immune priming, will be addressed in future studies. One of the limitations of the study is the narrow focus on CD8+ cells that neglects the complexity of immune contexture and sometimes contradictory roles they may have on progression and rejection of different tumor types. Nonetheless, by focusing on activated T cells, ¹⁸F-FARA-G may indirectly report on the behavior of other major players and thus immune activity of the TME, especially in tumor types for which strong evidence supports the positive predictive value of CD8+ cells, such as breast and head and neck cancers. The ability of ¹⁸F-FARA-G PET to assess the location and function of CD8+ cells, as well as immune activity within tumors post immune priming therapy warrants further investigation into its utility for patient selection, evaluation of optimal time to deliver immunotherapies, and assessment of combinatorial therapy approaches.

KEY POINTS

QUESTION: Can [¹⁸F]F-AraG PET be used to profile CD8 status of tumors and evaluate immunomodulation caused by chemotherapy?

PERTINENT FINDINGS: In a panel of syngeneic tumor models, a statistically significant correlation was found between the intratumoral [¹⁸F]F-AraG signal and the number of CD8+ PD-1+ cells. In addition, a statistically significant increase in signal post immune-priming oxaliplatin/cyclophosphamide treatment was observed in MC38 and A9F1 models.

IMPLICATIONS FOR PATIENT CARE: The ability of [¹⁸F]F-AraG PET to assess the location and function of CD8+ cells, as well as immune activity within tumors post immune priming therapy may prove useful in patient selection, evaluation of optimal time to deliver immunotherapies, and assessment of combinatorial therapy approaches.

REFERENCES

1. Junttila MR, de Sauvage FJ. Influence of tumour micro-environment heterogeneity on therapeutic response. *Nature*. 2013;501:346-354.
2. Binnewies M, Roberts EW, Kersten K, et al. Understanding the tumor immune microenvironment (TIME) for effective therapy. *Nat Med*. 2018;24:541-550.
3. Fridman WH, Zitvogel L, Sautes-Fridman C, Kroemer G. The immune contexture in cancer prognosis and treatment. *Nat Rev Clin Oncol*. 2017;14:717-734.
4. Chen DS, Mellman I. Elements of cancer immunity and the cancer-immune set point. *Nature*. 2017;541:321-330.
5. Ott PA, Hodi FS, Kaufman HL, Wigginton JM, Wolchok JD. Combination immunotherapy: a road map. *J Immunother Cancer*. 2017;5:16.
6. Casares N, Pequignot MO, Tesniere A, et al. Caspase-dependent immunogenicity of doxorubicin-induced tumor cell death. *J Exp Med*. 2005;202:1691-1701.
7. Lake RA, Robinson BW. Immunotherapy and chemotherapy--a practical partnership. *Nat Rev Cancer*. 2005;5:397-405.
8. Galluzzi L, Buque A, Kepp O, Zitvogel L, Kroemer G. Immunological effects of conventional chemotherapy and targeted anticancer agents. *Cancer Cell*. 2015;28:690-714.
9. Xin Yu J, Hodge JP, Oliva C, Neftelinov ST, Hubbard-Lucey VM, Tang J. Trends in clinical development for PD-1/PD-L1 inhibitors. *Nat Rev Drug Discov*. 2020;19:163-164.
10. Voorwerk L, Slagter M, Hurlings HM, et al. Immune induction strategies in metastatic triple-negative breast cancer to enhance the sensitivity to PD-1 blockade: the TONIC trial. *Nat Med*. 2019;25:920-928.
11. Ronald JA, Kim BS, Gowrishankar G, et al. A PET Imaging Strategy to Visualize Activated T Cells in Acute Graft-versus-Host Disease Elicited by Allogeneic Hematopoietic Cell Transplant. *Cancer Res*. 2017;77:2893-2902.
12. Franc BL, Goth S, MacKenzie J, et al. In Vivo PET Imaging of the Activated Immune Environment in a Small Animal Model of Inflammatory Arthritis. *Mol Imaging*. 2017;16:1536012117712638.

13. Levi J, Lam T, Goth SR, et al. Imaging of Activated T Cells as an Early Predictor of Immune Response to Anti-PD-1 Therapy. *Cancer Research*. 2019;79:3455-3465.
14. Eisenbach L, Segal S, Feldman M. MHC imbalance and metastatic spread in Lewis lung carcinoma clones. *Int J Cancer*. 1983;32:113-120.
15. Mosely SI, Prime JE, Sainson RC, et al. Rational Selection of Syngeneic Preclinical Tumor Models for Immunotherapeutic Drug Discovery. *Cancer Immunol Res*. 2017;5:29-41.
16. Lechner MG, Karimi SS, Barry-Holson K, et al. Immunogenicity of murine solid tumor models as a defining feature of in vivo behavior and response to immunotherapy. *J Immunother*. 2013;36:477-489.
17. Simon S, Labarriere N. PD-1 expression on tumor-specific T cells: Friend or foe for immunotherapy? *Oncoimmunology*. 2017;7:e1364828.
18. Pfirschke C, Engblom C, Rickelt S, et al. Immunogenic Chemotherapy Sensitizes Tumors to Checkpoint Blockade Therapy. *Immunity*. 2016;44:343-354.
19. Gooden MJ, de Bock GH, Leffers N, Daemen T, Nijman HW. The prognostic influence of tumour-infiltrating lymphocytes in cancer: a systematic review with meta-analysis. *Br J Cancer*. 2011;105:93-103.
20. Alam IS, Mayer AT, Sagiv-Barfi I, et al. Imaging activated T cells predicts response to cancer vaccines. *J Clin Invest*. 2018;128:2569-2580.
21. Larimer BM, Wehrenberg-Klee E, Dubois F, et al. Granzyme B PET Imaging as a Predictive Biomarker of Immunotherapy Response. *Cancer Res*. 2017;77:2318-2327.
22. Antonios JP, Soto H, Everson RG, et al. Detection of immune responses after immunotherapy in glioblastoma using PET and MRI. *Proc Natl Acad Sci U S A*. 2017;114:10220-10225.
23. Tavare R, Escuin-Ordinas H, Mok S, et al. An Effective Immuno-PET Imaging Method to Monitor CD8-Dependent Responses to Immunotherapy. *Cancer Res*. 2016;76:73-82.
24. Pages F, Mlecnik B, Marliot F, et al. International validation of the consensus Immunoscore for the classification of colon cancer: a prognostic and accuracy study. *Lancet*. 2018;391:2128-2139.
25. Pearce EL, Poffenberger MC, Chang CH, Jones RG. Fueling immunity: insights into metabolism and lymphocyte function. *Science*. 2013;342:1242454.

- 26.** Rotman J, Koster BD, Jordanova ES, Heeren AM, de Gruijl TD. Unlocking the therapeutic potential of primary tumor-draining lymph nodes. *Cancer Immunol Immunother.* 2019;68:1681-1688.
- 27.** Buck MD, O'Sullivan D, Klein Geltink RI, et al. Mitochondrial Dynamics Controls T Cell Fate through Metabolic Programming. *Cell.* 2016;166:63-76.
- 28.** Deng SM, Zhang W, Zhang B, Chen YY, Li JH, Wu YW. Correlation between the Uptake of F-18-Fluorodeoxyglucose (F-18-FDG) and the Expression of Proliferation-Associated Antigen Ki-67 in Cancer Patients: A Meta-Analysis. *Plos One.* 2015;10.
- 29.** Thommen DS, Koelzer VH, Herzig P, et al. A transcriptionally and functionally distinct PD-1(+) CD8(+) T cell pool with predictive potential in non-small-cell lung cancer treated with PD-1 blockade. *Nat Med.* 2018;24:994-1004.
- 30.** Scurr M, Pembroke T, Bloom A, et al. Low-Dose Cyclophosphamide Induces Antitumor T-Cell Responses, which Associate with Survival in Metastatic Colorectal Cancer. *Clin Cancer Res.* 2017;23:6771-6780.

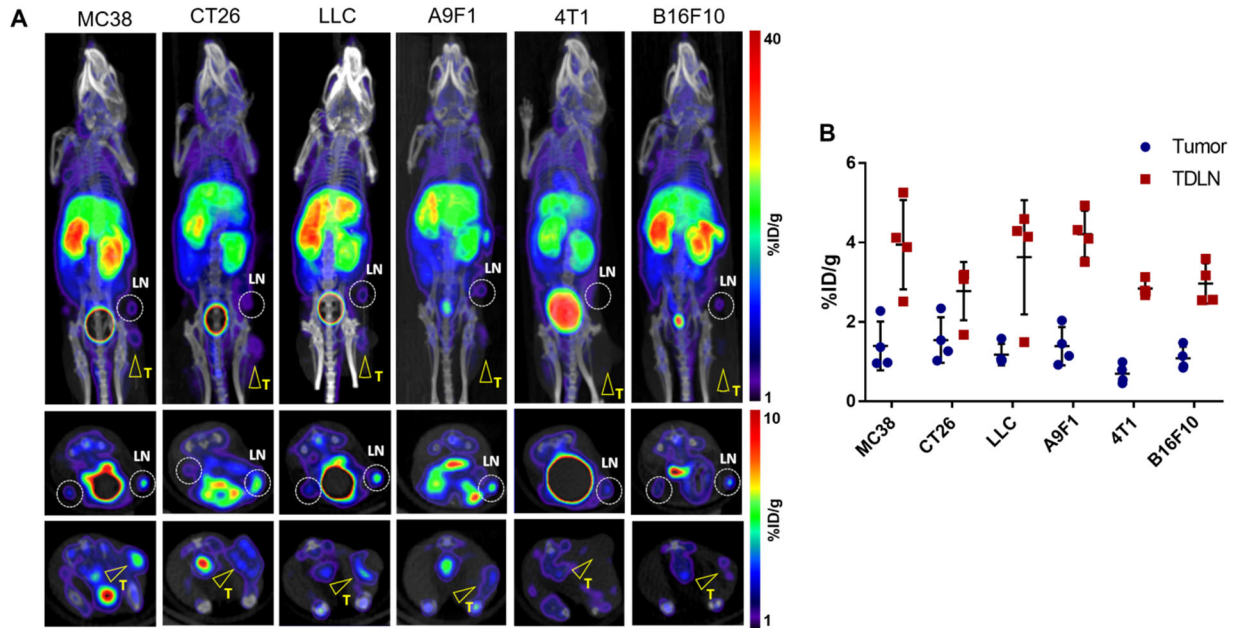


Figure 1. ^{18}F -FaraG imaging of different syngeneic tumor models. **A.** Both intratumoral (yellow arrows) and intranodal (white circles) signal varied between different tumor types. The location of the intratumoral signal showed several patterns, from signal present in the core (MC38 and A9F1) through halo-like (CT26) to signal present only at the margin (LLC, B16F10). Ring effect as observed in the bladder signifies a saturated signal. **B.** Intratumoral signal intensity showed variation between different tumor types and between individual mice of the same tumor type. The signal in the TDLNs was higher than the signal in the tumors and showed variability between different tumor types and individual mice ($n=4$ for each tumor type, error bars represent standard deviations).

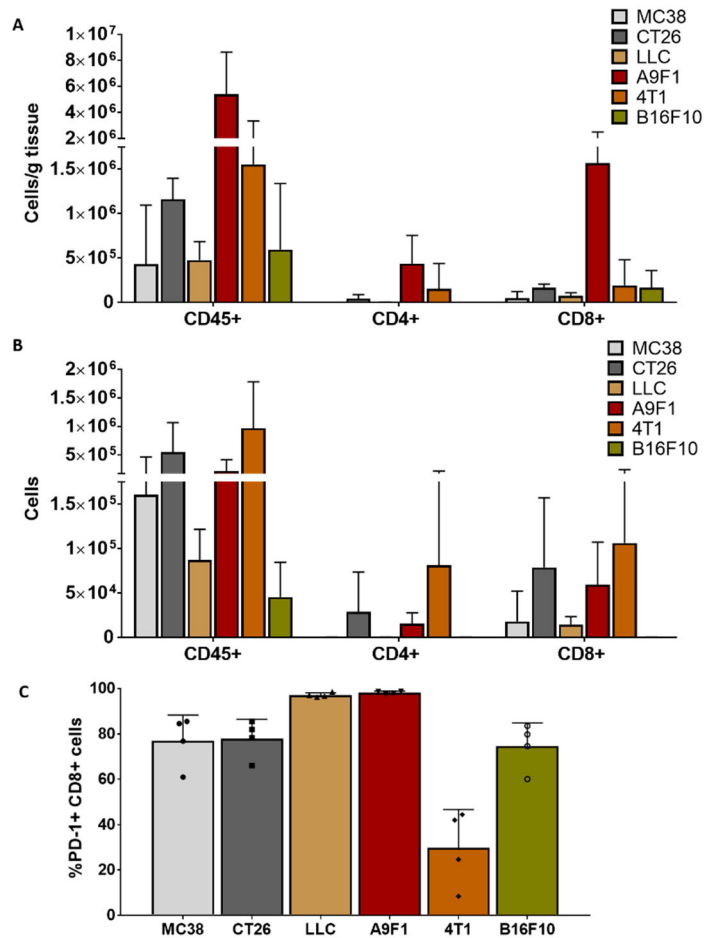


Figure 2. Evaluation of different syngeneic tumor models. **A.** The highest density of total lymphocytes, CD4⁺ and CD8⁺ cells was found in the smallest tumors, A9F1. **B.** The highest number of lymphocytes were isolated from the largest tumors, 4T1. **D.** Percentage of CD8 cells that expressed PD-1 varied between different tumor types. In LLC and A9F1 tumors, over 97 % of CD8 cells were found to be PD-1 positive, while in 4T1 tumors less than 30 % of CD8 cells were positive for PD-1 (n=4 for each tumor type, error bars represent standard deviations).

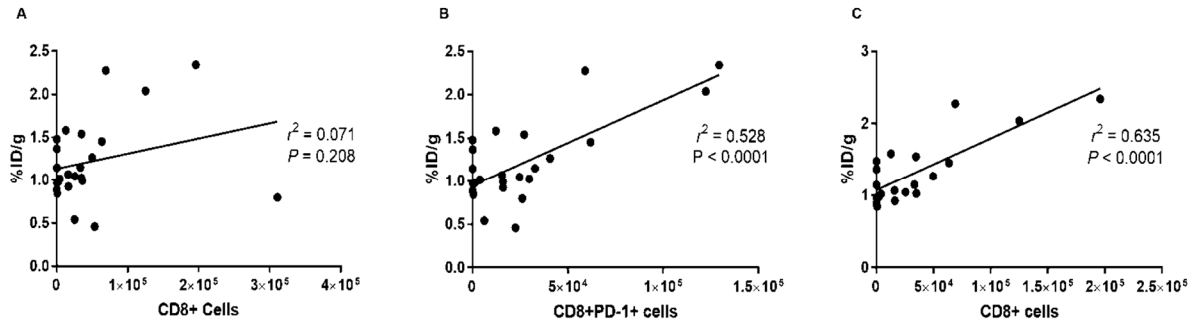


Figure 3. Correlation of the ^{18}F -FArArG signal with the number of CD8 cells present in the TME. **A.** The ^{18}F -FArArG signal showed no correlation with the number of intratumoral CD8+ cells. **B.** The ^{18}F -FArArG signal showed statistically significant correlation with the number of CD8+PD-1+ cells. **C.** Exclusion of 4T1 cells for which PD-1 expression indicated dysfunction led to statistically significant correlation between the ^{18}F -FArArG signal and the number of CD8+ cells.

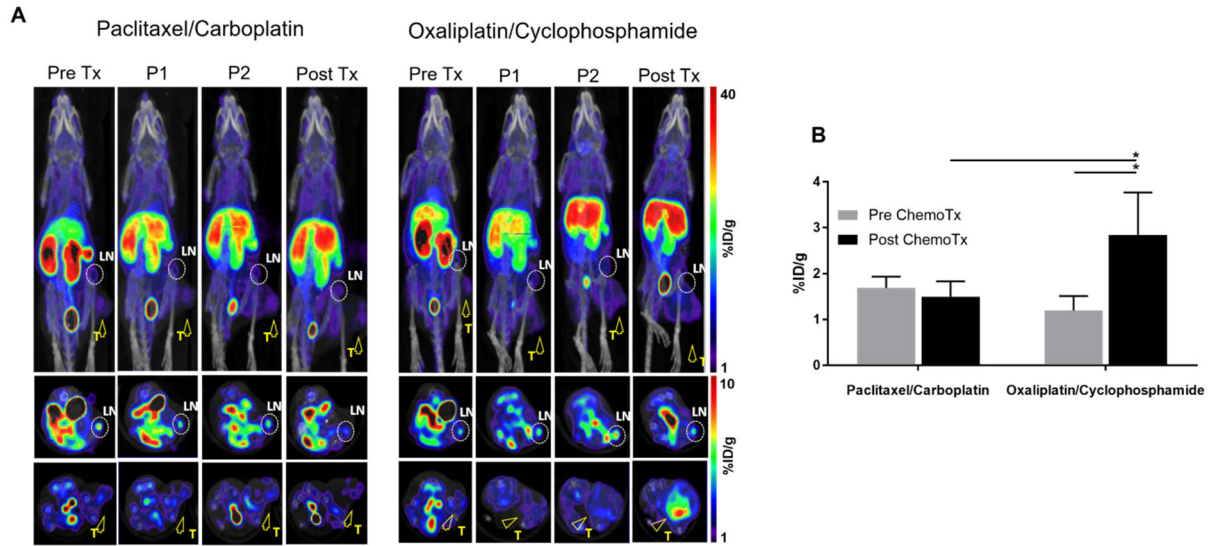


Figure 4. ^{18}F -FAraG longitudinal imaging of MC38 bearing mice undergoing chemotherapy. The chemotherapy was administered once a week for two weeks. Mice were imaged one day before the start of therapy (Pre Tx) and then 3 (P1) and 6 (P2) days after the first, and 3 days after the second chemotherapy administration (Post Tx). **A.** Paclitaxel/carboplatin treatment did not lead to appreciable changes in signal intensity. Dramatic increase in signal intensity was detected after two oxaliplatin/cyclophosphamide injections. White circles indicate tumor draining lymph nodes, yellow arrows point to tumors. **B.** The ^{18}F -FAraG signal detected post oxaliplatin/cyclophosphamide treatment was significantly different than the pre therapy signal as well as the signal post paclitaxel-carboplatin treatment ($n=4$ for each group, error bars represent standard deviation).

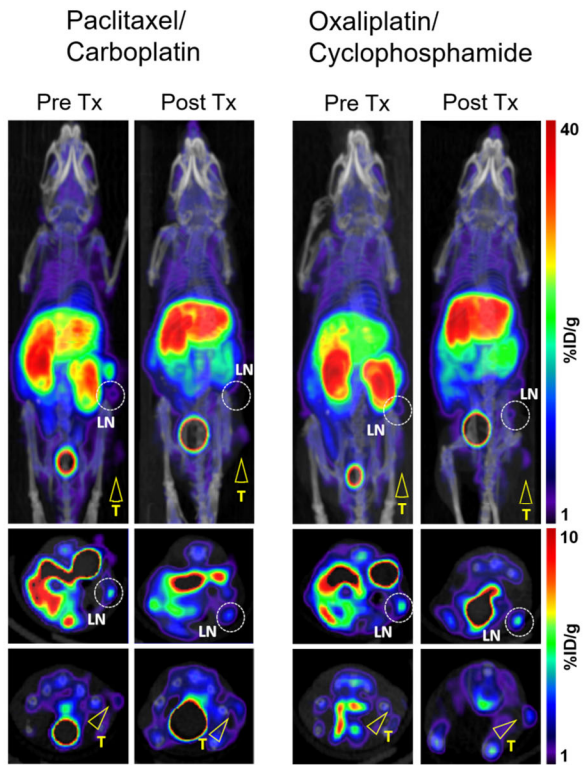
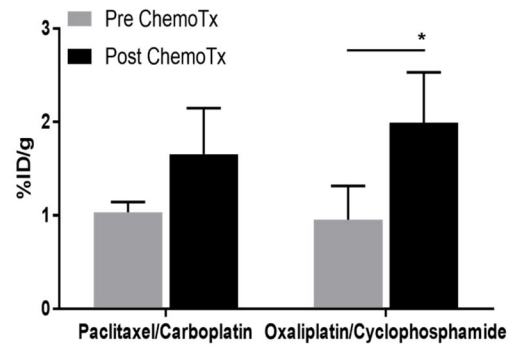
A**B**

Figure 5. ^{18}F -FARA G imaging of A9F1 bearing mice undergoing chemotherapy. **A.** Paclitaxel/carboplatin treatment showed a trend towards an increase in signal. Oxaliplatin/cyclophosphamide treatment led to an increase in intratumoral signal. White circles indicate tumor draining lymph nodes, yellow arrows point to tumors. **B.** The signal detected post oxaliplatin/cyclophosphamide treatment was significantly different than the pre therapy signal, but not the signal post paclitaxel-carboplatin treatment ($n=4$ for each group, error bars represent standard deviation).

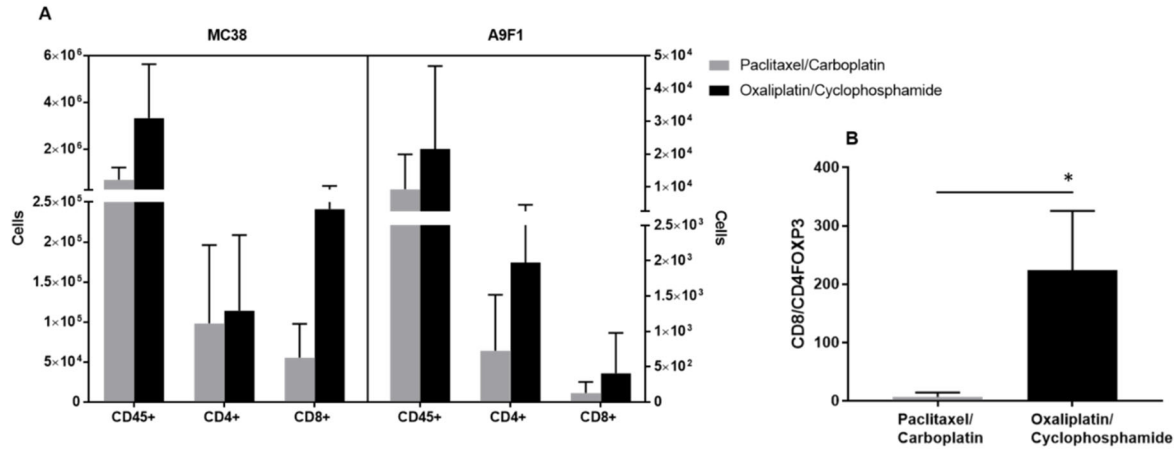
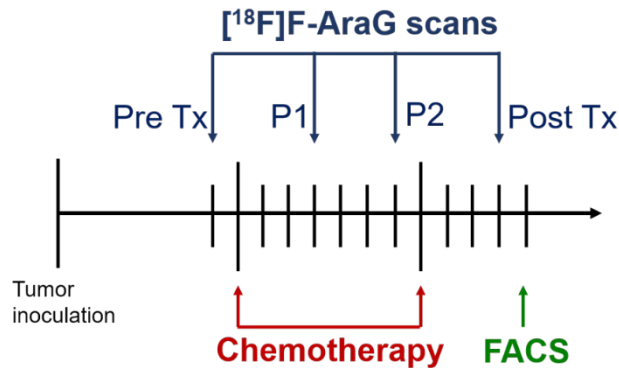


Figure 6. Lymphocyte profile of the MC38 and A9F1 tumors post chemotherapy. **A.** In MC38 tumors, oxaliplatin/cyclophosphamide treatment led to an increase in total lymphocytes and number of CD8+ cells. In A9F1 tumors, oxaliplatin/cyclophosphamide treatment led to an increase in total lymphocytes and number of CD4+ cells. **B.** In MC38 tumors, the ratio of CD8+ to CD4+FOXP3+ cells in the oxaliplatin/cyclophosphamide group was 27X higher than in the paclitaxel/carboplatin treated mice. (n=4 for each group, error bars represent standard deviation).

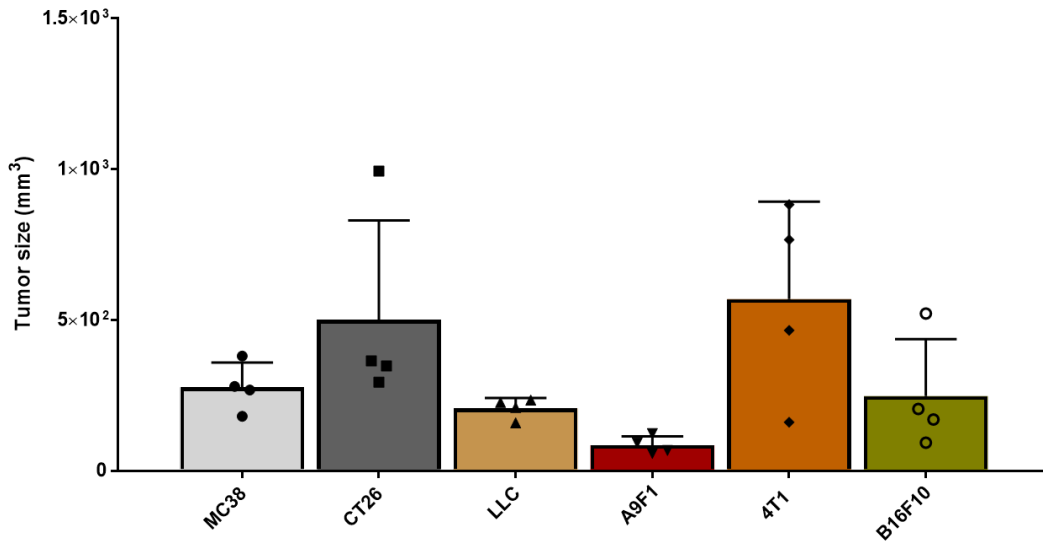
Supplemental Information



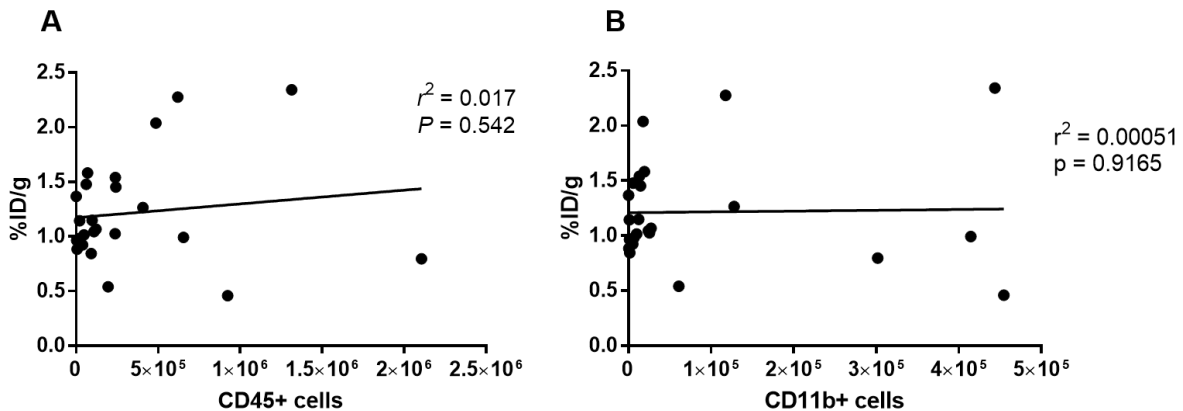
Supplemental Fig. 1. ^{18}F -AraG longitudinal imaging of MC38 bearing mice undergoing chemotherapy. The chemotherapy was administered once a week for two weeks. Mice were imaged one day before the start of therapy (Pre Tx) and then 3 (P1) and 6 (P2) days after the first, and 3 days after the second chemotherapy administration (Post Tx).

Marker	Fluorochrome	Clone	Company
CD45	Alexa Fluor 700	30-F11	Biolegend 103128
CD4	APC Cy7	GK1.5	Biolegend 100414
CD8	PerCP	53-6.7	Biolegend 100732
PD-1	Brilliant Violet 605	29F.1A12	Biolegend 135220
FoxP3	PE	150D	Biolegend 320008

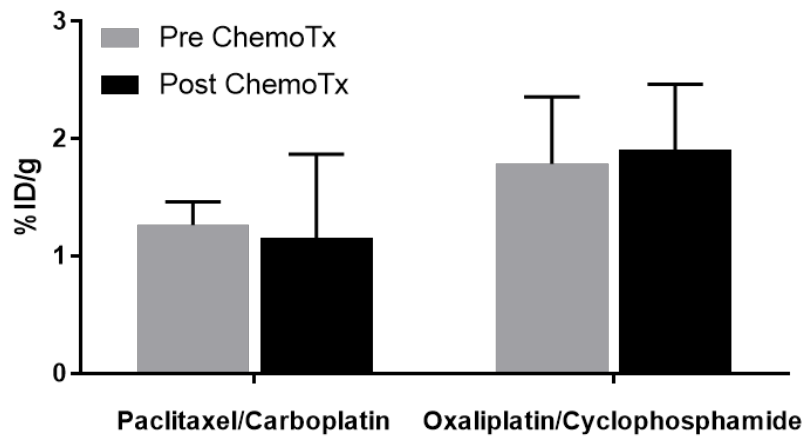
Supplemental Table 1. Antibodies used for FACS analysis of tumor infiltrating lymphocytes



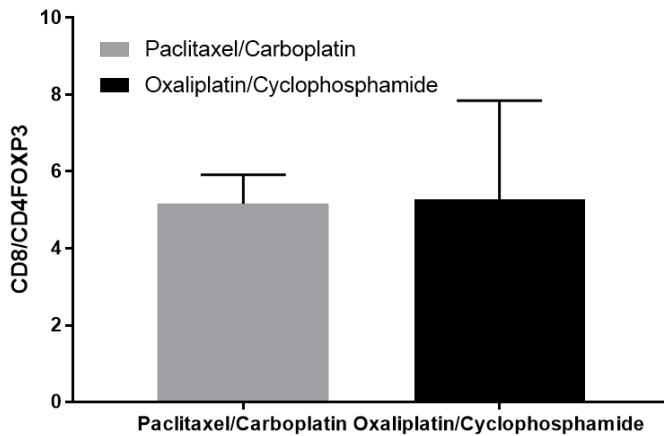
Supplemental Fig. 2. Tumor size prior to imaging differed between different tumor types and individual mice. The smallest sizes were recorded A9F1 tumors and the largest for 4T1 model.



Supplemental Fig. 3. Correlation of the [¹⁸F]F-AraG signal with the number of immune cells present in the TME. **A.** The [¹⁸F]F-AraG signal showed no correlation with the number of total lymphocytes found in the TME. **B.** The [¹⁸F]F-AraG signal showed no correlation with the number of CD11b+ cells found in the TME. CD11b is marker expressed on a variety of cells including macrophages, granulocytes and NK cells.



Supplemental Fig.4. The effects of chemotherapy in 4T1 tumor model. Neither paclitaxel/carboplatin or oxaliplatin/cyclophosphamide treatment led to a significant increase in [¹⁸F]F-AraG signal post therapy.



Supplemental Fig. 5. The effects of chemotherapy on the CD8/CD4FOXP3 ratio in A9F1 tumor model. The ratio of CD8+ to CD4FOXP3 cells was not significantly different between the groups of mice treated with paclitaxel/carboplatin and oxaliplatin/cyclophosphamide.